PLASMA DYNAMICS

VII. PLASMA PHYSICS*

Academic and Research Staff

Prof. S. C. Brown
Prof. W. P. Allis
Prof. J. C. Ingraham
Dr. G. Lampis
J. J. McCarthy
E. M. Mattison
W. J. Mulligan
F. Y-F. Tse

Graduate Students

M. L. Andrews
D. L. Flannery
E. V. George
P. W. Jameson
R. L. Kronquist
D. T. Llewellyn-Jones
G. L. Rogoff
D. W. Swain

A. ION-WAVE INSTABILITY IN A STEADY-STATE DISCHARGE

Following is a calculation of an ion-wave instability that can occur in a steady-state discharge in which no electric currents exist. The calculation assumes that all other plasma instabilities are absent so that to observe this instability experimentally conditions must be accordingly adjusted.

The plasma is assumed weakly ionized so that electron-ion collisions are negligible. The starting equations are the conservation of particle and momentum equations for electrons and ions and Poisson's equation:

$$\frac{\partial n_e}{\partial t} + \vec{\nabla} \cdot \overrightarrow{n_e v_e} = n_e S(T) \tag{1}$$

$$\frac{\partial}{\partial t} \overrightarrow{n_e v_e} + \frac{\gamma_e kT}{m_e} \overrightarrow{\nabla n_e} + \frac{n_e e}{m_e} (-\nabla\phi + \vec{v}_e \times \vec{B}) = -n_e \vec{v}_e \nu_e \tag{2}$$

$$\frac{\partial n_+}{\partial t} + \vec{\nabla} \cdot \overrightarrow{n_+ v_+} = n_e S(T) \tag{3}$$

$$\frac{\partial}{\partial t} \overrightarrow{n_+ v_+} - \frac{n_+ e}{m_+} (-\overrightarrow{\nabla\phi} + \vec{v}_+ \times \vec{B}) = -\overrightarrow{n_+ v_+} \nu_+ \tag{4}$$

$$\nabla^2 \phi = -\frac{e}{\epsilon_o} (n_+ - n_e), \tag{5}$$

where the ion temperature is neglected, and T is the electron temperature. The electrons are assumed to obey an equation of state

$$p_e = p_{eo} \left(\frac{n_e}{n_{eo}} \right)^{\gamma_e}. \tag{6}$$

*This work was supported by the United States Atomic Energy Commission under Contract AT(30-1)-1842.

The electron-atom and ion-atom collision frequencies are ν_e and ν_+, respectively. The particle source term $n_e S(T)$ balances the particle losses resulting from diffusion and recombination in a steady-state discharge. This term is generally a strongly increasing function of electron temperature so that if the electron temperature increases above the value corresponding to the steady state, production exceeds loss, and the ionization density grows. A low-frequency wave which modulates the electron temperature is thus coupled to the production of ionization through this source term.

Assume that the steady-state discharge is governed by ionization production through electron-atom ionizing collisions where the electrons have a Maxwellian velocity distribution. Assume that the ionization loss is due to diffusion to the walls of a cylindrical container of radius R and length L, having a magnetic field parallel to its axis. At steady state the production rate is[1]

$$n_s S(T_s) = n_s A T_s^{3/2} \, e^{-u_i/kT_s} \left(1 + \frac{u_i}{2kT_s}\right), \tag{7}$$

where A is a constant characteristic of the gas, and u_i is its ionization potential. The subscript "s" denotes steady state. The loss term, assuming the density to be distributed in the fundamental diffusion mode, is

$$(\vec{\nabla} \cdot \overrightarrow{n_e v_e})_s = n_s \frac{\mu_+ kT_s}{e} \left(\frac{\left(\frac{2.4}{R}\right)^2}{\left(1 + \mu_+ \mu_e B^2\right)} + \left(\frac{\pi}{L}\right)^2 \right), \tag{8}$$

where $\mu_+ = \frac{e}{m\nu_+}$ and $\mu_e = \frac{e}{m\nu_e}$ are the ion and electron mobilities, respectively. The equality of (7) and (8) determines T_s in steady-state discharge theory, and corresponds to the zero-order solution of (1) and (4). We assume that a small amplitude wave causes deviations from the steady state: $n_e = n_s + n_{e1}$, $n_+ = n_s + n_{+1}$, $T = T_s + T_1$, and we linearize (1) and (4). We also assume that the tube radius is much greater than the wavelength of the disturbance so that zero-order density gradient effects on the wave propagation are negligible (except as they determine the loss of particles to the walls due to diffusion). This gives

$$\frac{\partial n_{e1}}{\partial t} + n_s \vec{\nabla} \cdot \vec{v}_e = \frac{\partial n_{+1}}{\partial t} + n_s \vec{\nabla} \cdot \vec{v}_+ =$$

$$n_s \left(- \frac{\mu_+ kT}{e} \left[\frac{\left(\frac{2.4}{R}\right)^2}{1 + \mu_+ \mu_e B^2} + \left(\frac{\pi}{L}\right)^2 \right] + AT^{3/2} \, e^{-u_i/kT} \left(1 + \frac{u_i}{2kT}\right) \right), \tag{9}$$

where $\vec{v}_e$ and $\vec{v}_+$ are due only to the wave and not to the density gradients. Using Eqs. 7 and 8 and the fact that they are equal for $T = T_s$, we linearize the right-hand side of Eq. 9 to obtain

$$\frac{\partial n_{e1}}{\partial t} + n_s \vec{\nabla}\cdot\vec{v}_e = \frac{\partial n_{+1}}{\partial t} + n_s \vec{\nabla}\cdot\vec{v}_+ =$$

$$n_s \frac{\mu_+ kT_s}{e}\left(\frac{\left(\frac{2.4}{R}\right)^2}{\left(1+\mu_+\mu_e B^2\right)} + \left(\frac{\pi}{L}\right)^2\right)\left(-1 + \frac{\frac{3}{2} + \frac{5}{4}\frac{u_i}{kT_s} + \frac{u_i^2}{2(kT_s)^2}}{\left(1+\frac{u_i}{2kT_s}\right)}\right)\frac{T_1}{T_s}.$$

Using $p_e = n_e kT$ and Eq. 6, we obtain $T_1/T_s \cong (\gamma_e - 1)n_{e1}/n_s$, and assuming $u_i/kT_s \gg 1$, Eq. 10 becomes

$$\frac{\partial n_{e1}}{\partial t} + n_s \vec{\nabla}\cdot\vec{v}_e = \frac{\partial n_{+1}}{\partial t} + n_s \vec{\nabla}\cdot\vec{v}_+ = \beta n_{e1}, \tag{11}$$

where

$$\beta \equiv (\gamma_e - 1)\frac{\mu_+ u_i}{e}\left(\frac{\left(\frac{2.4}{R}\right)^2}{1+\mu_+\mu_e B^2} + \left(\frac{\pi}{L}\right)^2\right). \tag{12}$$

The coefficient β will lead to growth of low-frequency ion waves under conditions determined below. In solving the ion-wave problem we assume that

$$n_{e1} = \frac{\epsilon_o \phi}{e\lambda_D^2}, \tag{13}$$

where

$$\lambda_D^2 = \frac{\gamma_e kT_s \epsilon_o}{n_s e^2}. \tag{14}$$

Equation 13 is valid, provided the electrons can move freely along the magnetic field lines so as to neutralize the ion space charge. With this assumption and assuming $\vec{B} = \vec{B}_o$ we are left with only (3), (4), and (5) to solve with n_{+1}, $\vec{v}_+$, and ϕ the unknowns. Assuming that these quantities vary as $\exp\left[i(\omega t - \vec{k}_\perp\cdot\vec{r} - kz)\right]$, where the z-axis is parallel to and $\vec{k}_\perp$ perpendicular to $\vec{B}_o$ we obtain the dispersion relation

$$k_\perp^2\lambda_D^2\left(1+\frac{\omega_{p+}^2}{i\omega(i\omega+\nu_+)\left(1+\frac{\omega_{B+}^2}{(i\omega+\nu_+)^2}\right)}\right)+k^2\lambda_D^2\left(1+\frac{\omega_{p+}^2}{i\omega(i\omega+\nu_+)}\right),+\left(1-\frac{\beta}{i\omega}\right)=0 \tag{15}$$

where $\omega_{p+}^2=\frac{n_s e^2}{m_+\epsilon_o}$ is the square of the ion plasma frequency and $\omega_{B+}=\frac{eB_o}{m_+}$ is the ion cyclotron frequency. Assuming $\omega=\omega_r+i\omega_i$ and that k and $k_\perp$ are real allows us to determine the stability of the system, negative ω_i giving rise to instability. The equation in its general form is very difficult to solve and only one example will be treated at this time – that of ion-acoustic wave propagation parallel to $\vec{B}_o$ ($k_\perp=0$). We obtain from (15)

$$\omega_i=\nu_+-X+\sqrt{X^2-\nu_+X-\omega_r^2}, \tag{16}$$

where

$$X\equiv\frac{k^2\lambda_D^2\omega_{p+}^2}{\beta}.$$

For $\omega_i=0$ we obtain from Eq. 15

$$\omega_r^2=\frac{k^2\lambda_D^2\omega_{p+}^2}{1+k^2\lambda_D^2}-\nu_+^2. \tag{17}$$

Substituting (17) in (16), we find that for $\omega_i\leq 0$ we must have

$$\beta\geq\nu_+\left(1+k^2\lambda_D^2\right)\approx\nu_+ \tag{18}$$

By using Eq. 18 combined with Eq. 12, it is then possible for a given experiment to calculate at what pressure the first ion acoustic wave instabilities should appear, and from Eq. 17 it is possible to calculate their frequencies.

The damping for waves with $k_\perp\neq 0$ will be greater because of the ion cyclotron absorption, so that as pressure is decreased in a given experiment, the waves with $k_\perp=0$ will become unstable first.

J. C. Ingraham

References

1. S. C. Brown, Basic Data of Plasma Physics (John Wiley and Sons Ltd., New York, 1959), p. 289.

B. LASER BREAKDOWN EXPERIMENT

The laser breakdown experiment is proceeding (see Quarterly Progress Report No. 81, page 58). The pulse from the ruby laser has been stabilized to the power of 50 MW (2 J in 40 nsec). The gas is helium at 10.25 kg/cm^2 pressure.

The first part of the experiment was devoted to the determination of the transmission rate of the gas laser power (HeNe) through the plasma, with the aim of gaining knowledge of the absorption coefficient of the light at 6328 Å, and measuring the dimensions of the plasma during its evolution in time.

In measuring the transmission of the laser light, it is necessary to take care that the plasma acts as a negative lens on the gas-laser beam, spreading it out. To collect the beam while it is being spread out, and to measure the solid angle of the spreading in time, the geometry of the optics of the early measurements was modified (Fig. VII-1).

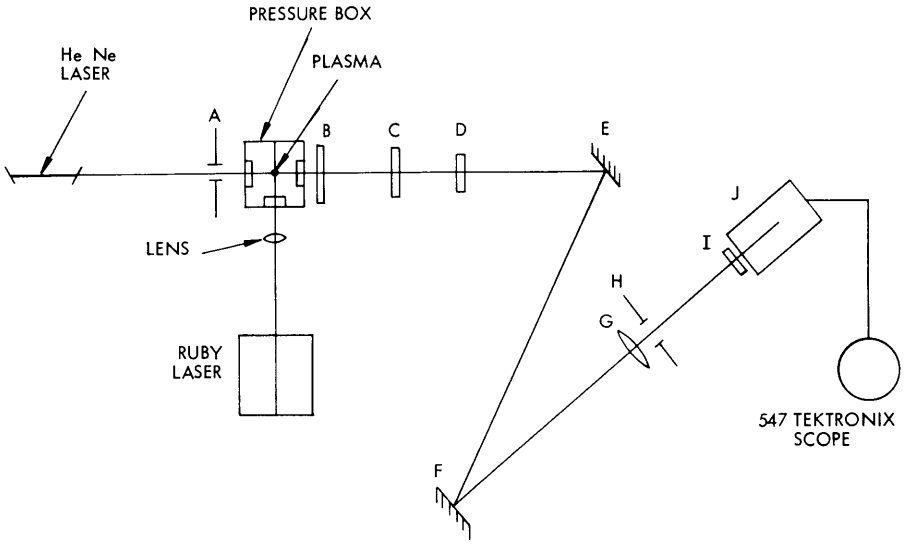

A. DIAPHRAGM (2 mm)
B. SHARP CUT OFF FILTER
C. POLARIZER
D. INTERFERENCE FILTER (30 Å BANDWIDTH)
F-E. SILVER REFLECTING MIRRORS
G. LENS 360 mm FOCAL LENGTH
H. ADJUSTABLE DIAPHRAGM
I. SHARP INTERFERENCE FILTER (5 Å BANDWIDTH)
J. RCA 6199 PHOTOMULTIPLIER TUBE

Fig. VII-1. Experimental arrangement for measuring density and absorption.

The diaphragm, A, brings the gas laser beam to a known diameter (2 mm). The sharp cutoff filter, B, eliminates the unwanted light from the plasma with frequency

over 5800 Å, while the rotatable polarizer, C, is set for maximum transmission for the already polarized gas-laser light, thereby favoring by a factor of two the competition between the gas laser light and the plasma emission (which is not polarized), at the same frequency within the band of the two interference filters, D and I, in cascade, both being tilted to peak transmission at 6328 Å.

The diaphragm, H, beyond the lens, G, (focal length 360 mm) can be adjusted in seven positions (f/5.6, f/8, f/11, f/16, f/22, f/32, 3 mm).

The photomultiplier tube is set in such a position that the image of the plasma through the lens, G, is focused on the photosensitive cathode.

The silvered mirrors, E and F, are used to extend the optical path up to the desired length. The optical path was optimized at a length of 183 cm between plasma and lens. Shorter paths favor the plasma emission toward the gas laser; longer paths cause the largest aperature of the diaphragm, I, to catch only a part of the light of the gas laser, which is spread out as a cone by the plasma lens and thus gives a false value of the transmission of the gas laser through the plasma.

With this arrangement, several sets of emission curves (plasma alone) and combination curves (gas laser and plasma) were taken, with different apertures of the diaphragm, H, used. Figures VII-2 and VII-3 show four different diaphragm situations; the geometry of the detection always allowed signals limited enough to prevent the photomultiplier tube from working in the nonlinear region.

From every combination curve, the corresponding emission curve was subtracted; in this way, a set of curves of transmission versus time of the gas laser was obtained for different solid angles of detection.

Figure VII-4 shows the set of absorption curves, for different times, between 175 and 630 nsec after breakdown. The quantity plotted on the ordinate is the transmission per unit solid angle; the quantity on the abscissa is the solid angle itself. (The solid angle is the one through which the adjustable diaphragm sees the plasma.)

It is clearly seen by the set of curves that at every time there is a solid angle where the curve becomes a straight line set at 45°; this means that all diaphragms on the 45° line get the whole laser beam (at the same time) and all of them measure the true transmission, while the smaller diaphragms out of the 45° line get only a part of the laser beam.

For longer times the plasma density slows down and the gas-laser beam approaches its natural divergence, and smaller diaphragms can catch it; this is shown by the movement of the knee on the transmission curves. Plotting the solid angle of the knee against time (Fig. VII-5), we find an exponential decay.

From the theory of a cylindrical plasma lens, the index of refraction of the

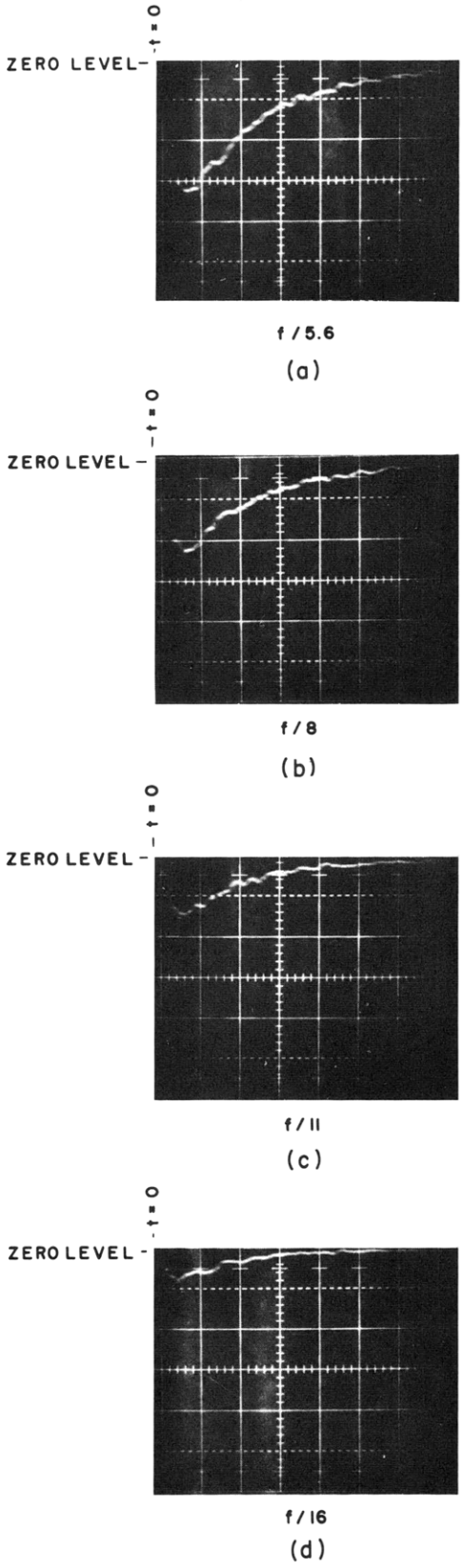

Fig. VII-2. Plasma emission. Vertical scale: 5 mV/div.
Horizontal scale: 100 nsec/div.

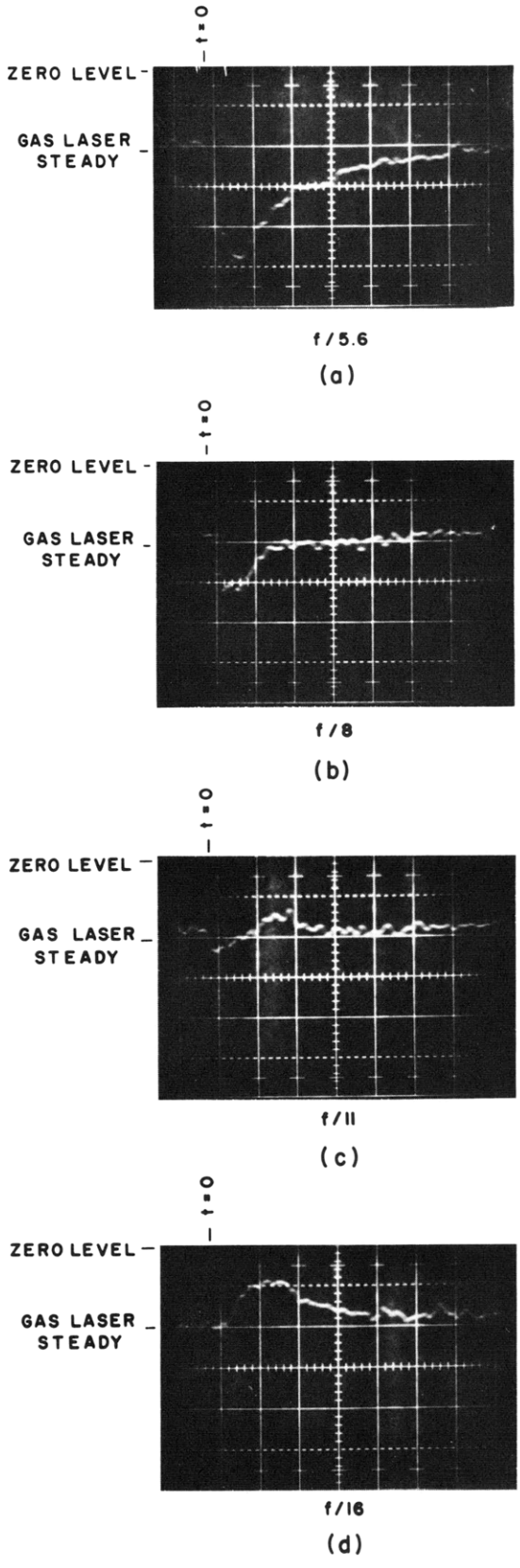

Fig. VII-3.

Combination curves (gas laser plus plasma emission). Vertical scale: 5 mV/div. Horizontal scale: 100 nsec/div.

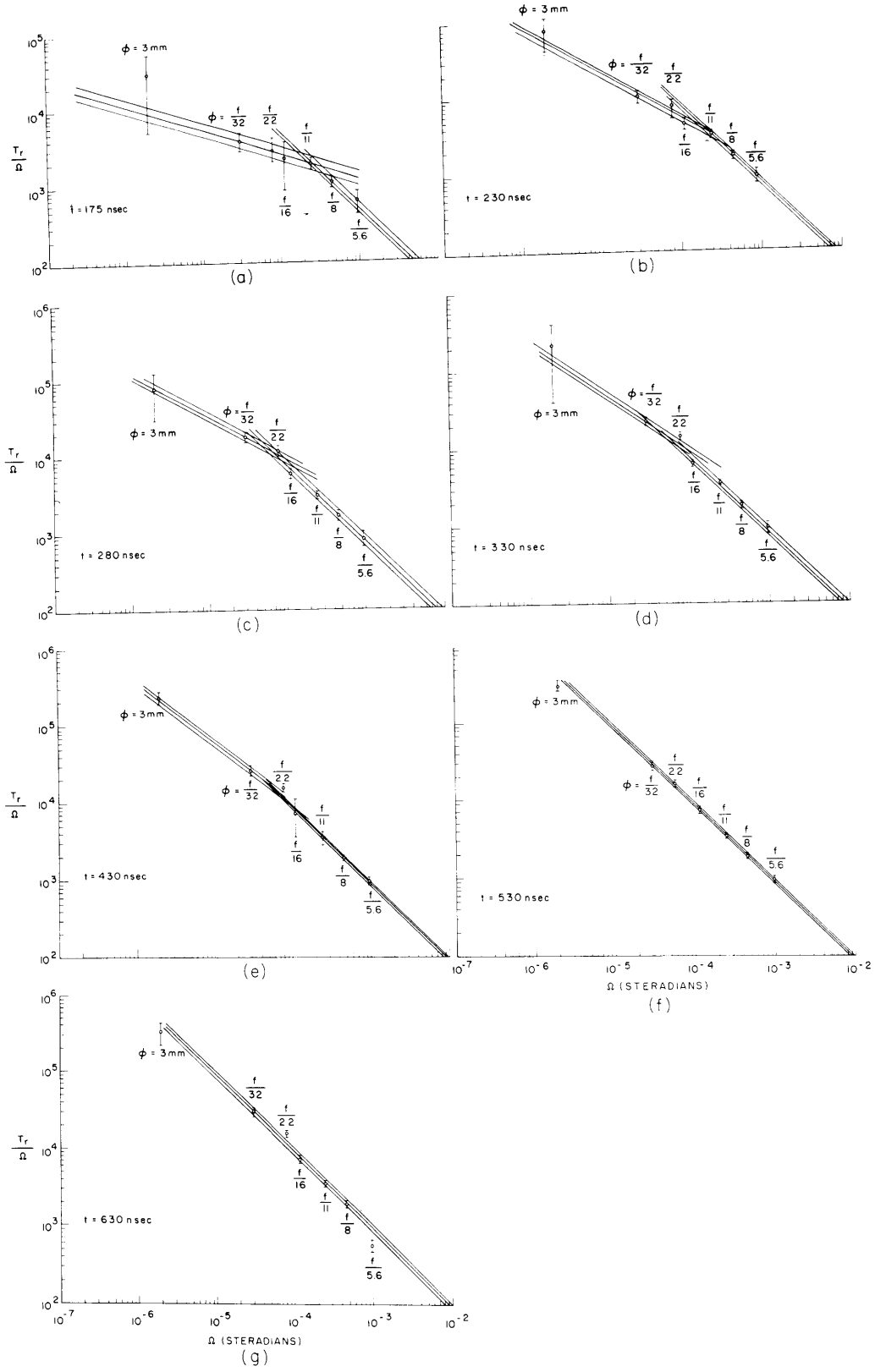

Fig. VII-4. Evolution of the gas-laser spreading and the transmission.

plasma is then immediately known in time (under the assumption that the plasma is uniform.)

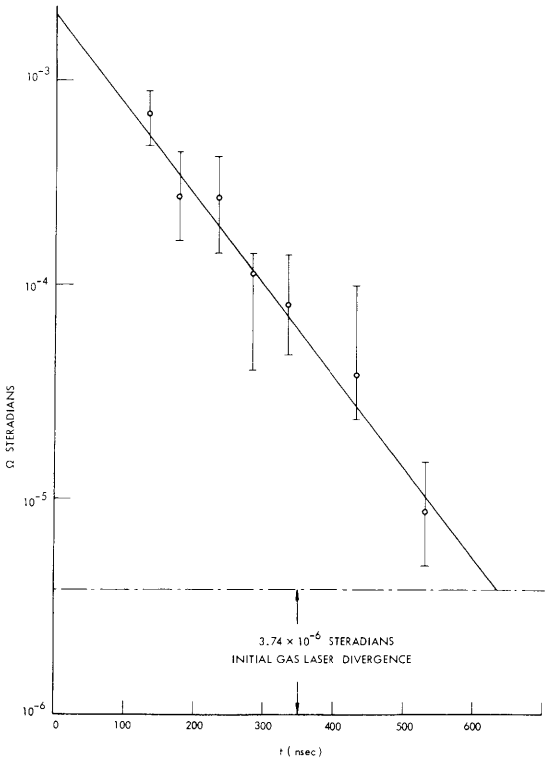

Fig. VII-5. Gas-laser spreading decay.

$$\frac{1}{r} = 1 + \frac{\theta_e - \theta_i}{2\left(\frac{P}{D} + \theta_i\right)},$$

where θ_e is the half-divergence of the gas laser as it comes out of the plasma (radiants), r is the index of refraction, P is the diameter of the incoming gas laser beam (2 mm), D is the diameter of the plasma (varying in time), and θ_i is the half-divergence (radiants) of the gas laser before entering the plasma.

From the index of refraction, the density follows immediately:

$$r = \left[1 - \left(\frac{\omega_p}{\omega}\right)^2\right]^{1/2} \quad ; \quad \omega_p = 56.45 \cdot 10^3 \cdot N^{1/2},$$

where ω is the frequency of the gas laser light, $2.975 \cdot 10^{15} \frac{\text{rad}}{\text{sec}}$, ω_p is the plasma frequency, and N is the density $\frac{\text{electrons}}{\text{cm}^3}$.

Figure VII-6 shows that the behavior of the density vs time from 100-500 nsec after breakdown is an exponential decay. The density is known within 30 per cent.

Keeping in mind that at a pressure of 10.25 kg/cm^2 the atom density is $2.5 \cdot 10^{20}$ in $\frac{\text{atoms}}{\text{cm}^3}$, we find at 100 nsec an average ionization degree of 23 per cent.

To find the density for earlier times, it is necessary to use a shorter optical path and thus catch the beam when it is more spread out. This could require a more powerful gas laser, having a power comparable with the emission from the plasma.

A correction of the gas-laser absorption curves was necessary because the gas-laser beams coming out of the lens meet the sharp filter at slightly different angles and result in different transmissions; by shining the gas laser alone, and moving it through known patterns on the surface of the lens at different known angles of incidence, a map of the transmission on all of the surface of the filter was made, thereby yielding a correction factor for every measurement taken with a different diaphragm size.

The error bars in the knee curves were obtained by taking different sets of data and

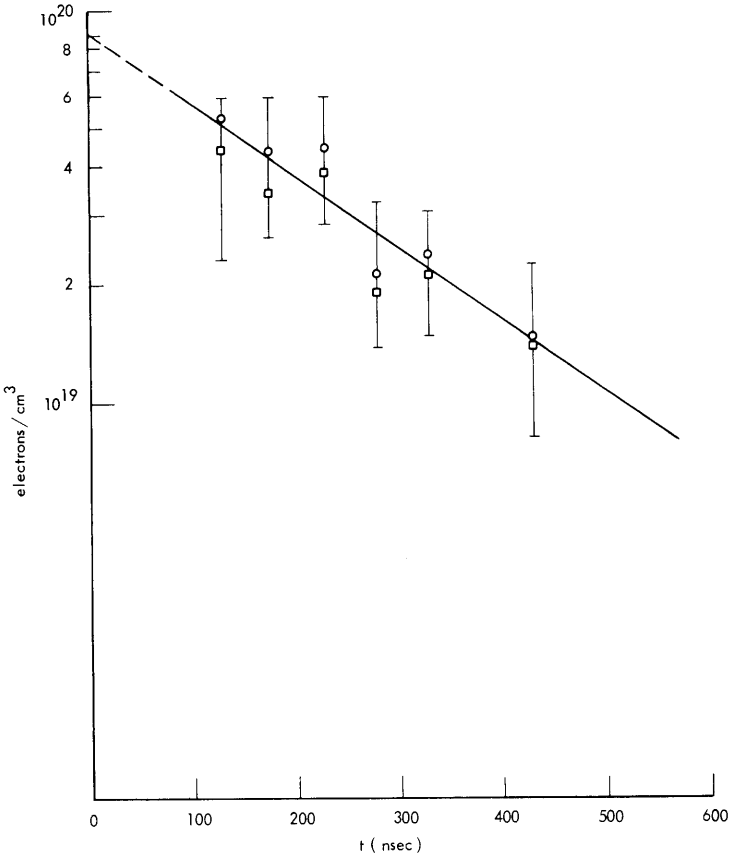

Fig. VII-6. Plasma-density decay.

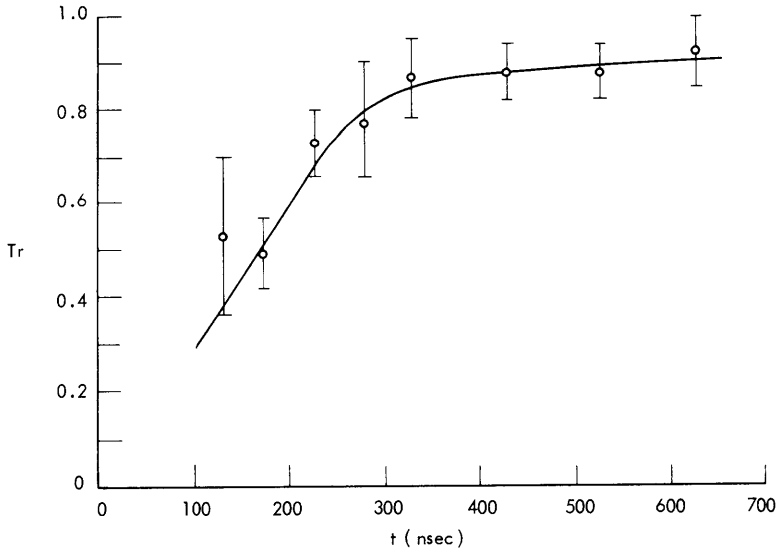

Fig. VII-7. Gas-laser transmission.

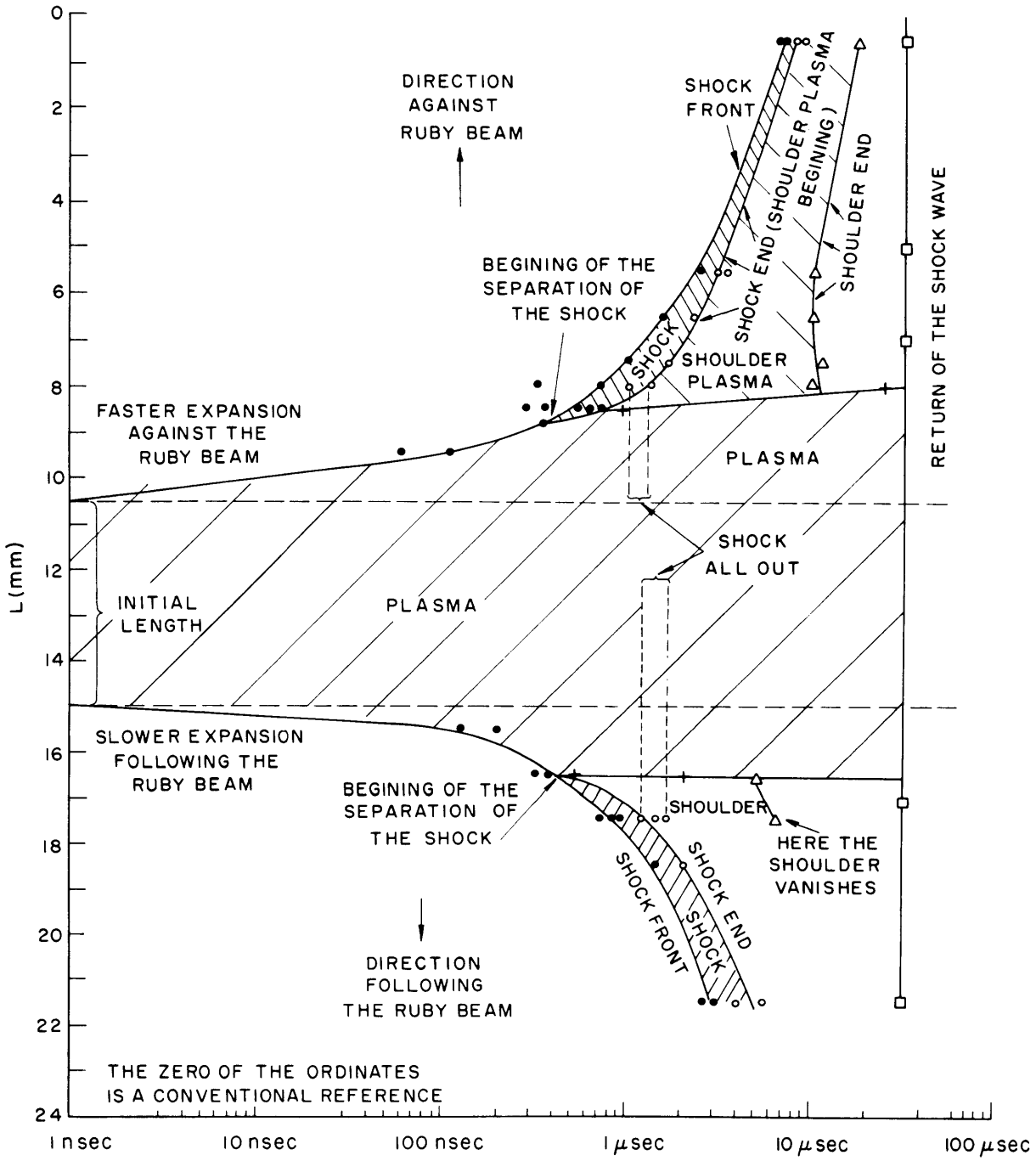

Fig. VII-8. Axial expansion of the plasma probing beam. Beam diameter: 1 mm. Ruby laser power: 50 MW.

keeping account of the noise of the gas laser. From the 45° points of the "knee-curves," it is possible to read the behavior of the transmission of the gas laser through the plasma as a function of time (Fig. VII-7); this quantity, together with the radius of the plasma, gives the absorption coefficient, which is necessary to get the temperature from the emission curves calibrated with the gas laser.[1]

To find the behavior of the length of the plasmas in time, small diaphragms (1-mm diameter) were inserted before and after the windows of the box where the plasma is produced; this gives the gas laser a known section and cuts down the emission from the plasma, so that only the absorption of the gas laser can be detected. The plasma was moved by known amounts along its axis with respect to the gas laser by moving the focussing lens along the ruby beam.

The delay in the beginning of the absorption related to the position of the plasma gives the information on the axial expansion.

Figure VII-8 shows the behavior of the length of the plasma up to 32 μsec. At ~500 nsec the plasma starts to throw out a shock wave from the two heads which produces a plasma itself after its own shoulder. Figure VII-9 shows the instant when the shock separates from the plasma (side of the plasma toward the lens), 1.1-1.3 μsec. Figure VII-10 shows the shock already separated from the initial blob and dragging the shoulder plasma.

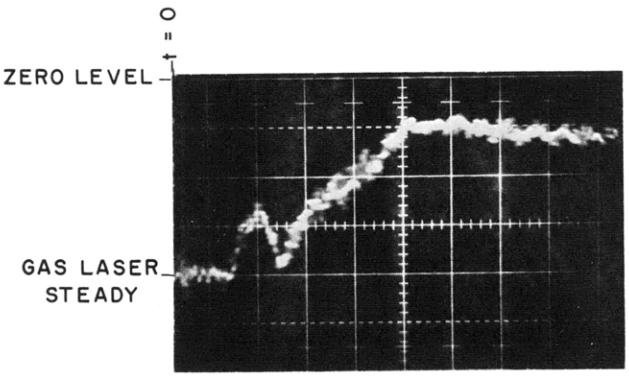

Fig. VII-9. Shock wave from the head of the plasma toward the lens. (Direction against the ruby beam.) Horizontal scale: 500 nsec/div. Vertical scale: 5 mV/div.

The initial length of the plasma is 4.5 mm; it grows to 7.9 mm in 500 nsec. While emitting the shock, the plasma cools strongly and the expansion rate slows down; at 1 μsec the length is 8 mm.

At 32 μsec after breakdown the shock waves emitted from the two heads of the cylinder of plasma are reflected back on the plasma by the walls of the box, and the plasma becomes enormously turbulent and inhomogeneous.

It can be seen from Fig. VII-8 that the plasma explodes mainly toward the focussing lens (direction against the ruby beam); the shock-wave velocity and the axial-expansion velocity of the plasma are faster in the direction against the lens, as predicted by the theory.[2] Also, the time when the shock is completely emitted is different from one head to the other head of the plasma, as seen from Fig. VII-8. Further work is in progress on this point.

The fact that the shock surrounding the plasma drags on ionized layer (shoulder plasma) warns us that in any temperature measurement made when this plasma is present (from 500 nsec after breakdown) the emission of this shoulder plasma itself should be taken into account. Figure VII-8 shows, too, the border of existence of this "shoulder" on both sides of the initial cylinder of plasma.

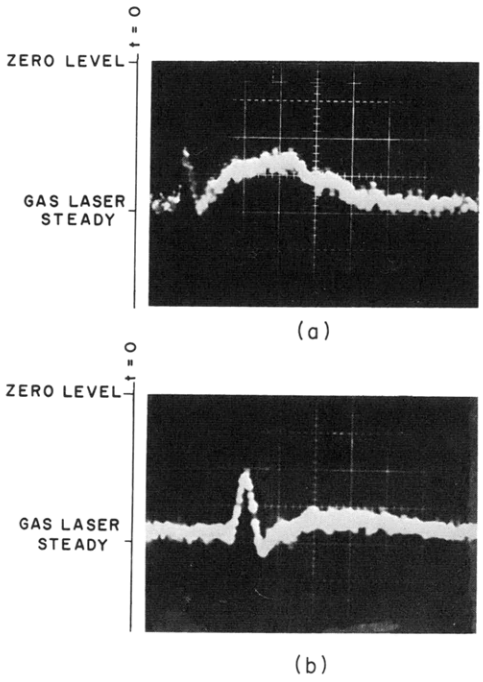

Fig. VII-10. Shock wave dragging its own shoulder plasma.

To measure the radial expansion of the plasma, a new geometry was set up (Fig. VII-11). By tilting the quartz slab before the box, it was possible to offset up and down the gas-laser beam with a precision up to 1/10 mm. The gas laser was then reset for every position with a second slab after the box. On the two sides of the box two vertical slits (1 mm wide, 2 cm long) were set up to let the gas-laser beam through and cut down the emission, and a small diaphragm was put before the detector (2-mm diameter). Again, the delay in the beginning of the absorption related to the position of the beam gives the information on the evolution in time of the radius of the plasma. The initial position is found when the plasma explodes at the surface of the gas-laser beam; by offsetting the beam of the first 4/10 mm, the first delay of 30 nsec is seen. Figure VII-12 shows the behavior of the radius growth from the initial value of 0.15 mm (focal spot of the lens) as a function of time.

The plasma throws out a radial shock wave whose position is shown, together with the position of its end, coincident with the beginning of the shoulder plasma. The separation of the shock from the plasma starts around 300 nsec after breakdown, and the shock is completely separated 1.2-1.5 μsec after breakdown.

The knowledge of the radius of the plasma is indispensable, in getting the index of refraction from the measurements of its lens effect on the gas-laser beam, and the absorption coefficient from the curve of transmission. When using the gas laser, both the length and the radius of the plasma are indispensable to compute the temperature from the calibrated emission curves and the absorption coefficient.

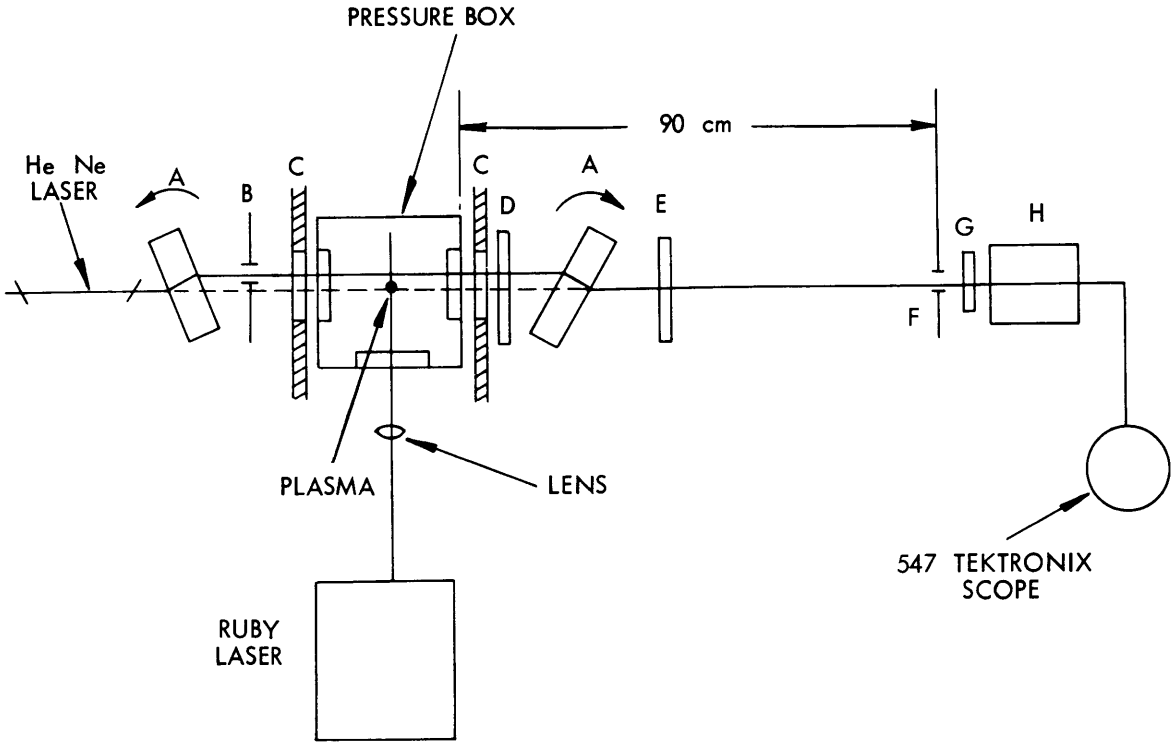

A. QUARTZ TILTABLE SLABS
B. VERTICALLY MOVABLE DIAPHRAGM
C. VERTICAL SLITS (1 mm. WIDE, 2 cm. LONG)
D. SHARP CUT OFF FILTER
E. POLARIZER
F. DIAPHRAGM (2 mm)
G. SHARP INTERFERENCE FILTER
H. RCA 6199 PHOTOMULTIPLIER TUBE

Fig. VII-11. Experimental arrangement for measuring the radial expansion of the plasma.

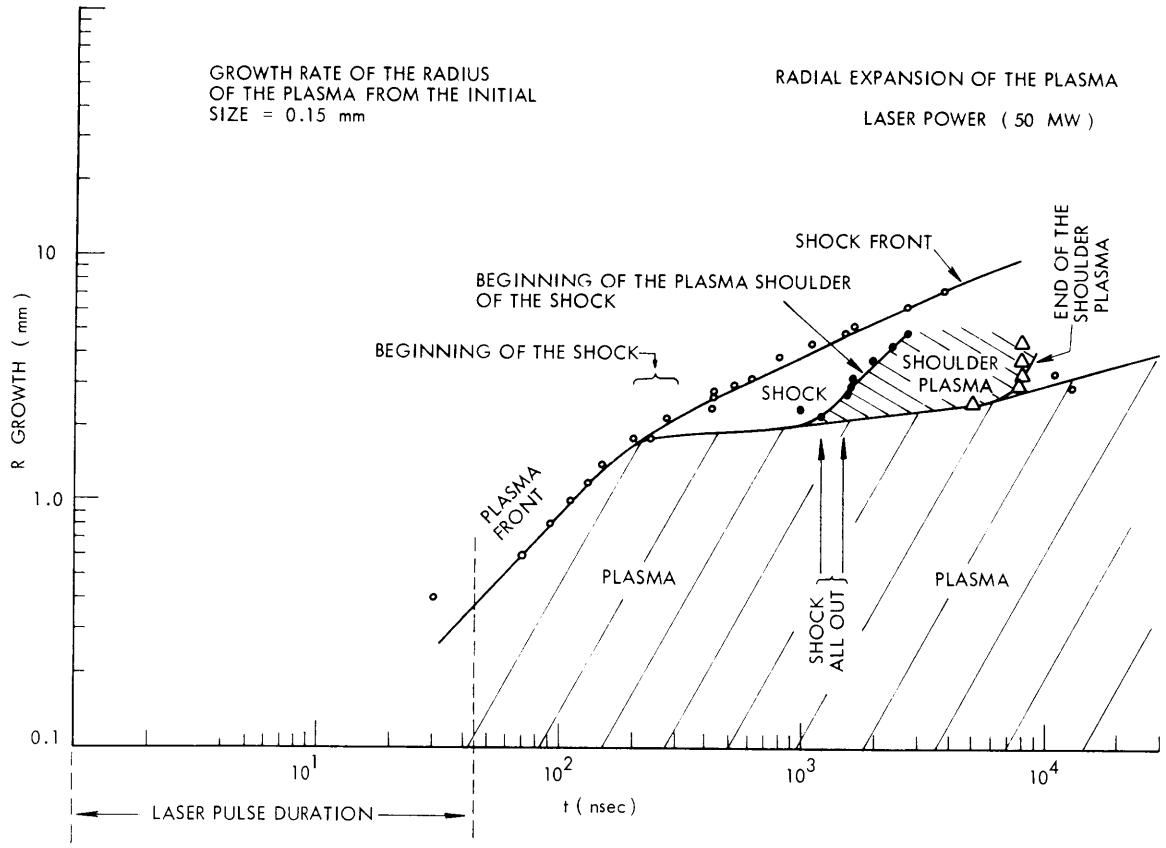

Fig. VII-12. Evolution of the radial expansion of the plasma.

The calibration of the emission curves taken with different diaphragm apertures, for optimizing with respect to angle effects on the sharp filter, has been carried out and computation of the temperature of the plasma is in progress.

G. Lampis

References

1. G. Lampis, "Laser Breakdown," Quarterly Progress Report No. 81, Research Laboratory of Electronics, M.I.T., April 15, 1966, pp. 58-61.
2. Yv. P. Raizer, Soviet Phys. – JETP, Vol. 21, No. 5, November 1965.
3. Yv. P. Raizer, Soviet Phys. – Usp., Vol. 22, No. 5, March-April 1966.

C. MICROWAVE SCATTERING FROM STANDING PLASMA WAVES

Observations of microwave scattering from density fluctuations in an electron-beam produced plasma[1] have continued. The nature of the fluctuations responsible for the scattering now seems quite clear. All of the experimental evidence indicates that the scattering is from plasma waves excited by the electron beam which reflect from the ends of the plasma column and form standing waves along the axis of the tube.

The experimental geometry and procedure are similar to those previously reported[1]; this report also contains references to the theory of density fluctuations and the scattering of electromagnetic waves from these fluctuations.

The present experiments were carried out in a plasma produced by firing an electron beam into un-ionized mercury vapor. The plasma tube was sealed off, and the vapor pressure of the mercury was determined by the temperature of the reservoir of liquid mercury. In all cases this temperature was held at 0°C, with the result that there was a vapor pressure of approximately 2×10^{-4} mm Hg. The electron gun was a focussed Pierce-type gun. The axis of the tube was aligned along a uniform magnetic field, but the gun was shielded from the field, so that the transverse energy of electrons emerging from the gun was increased as they entered the magnetic field. Since the beam electrons have some transverse energy, the axial velocity is expected to be close to, but somewhat

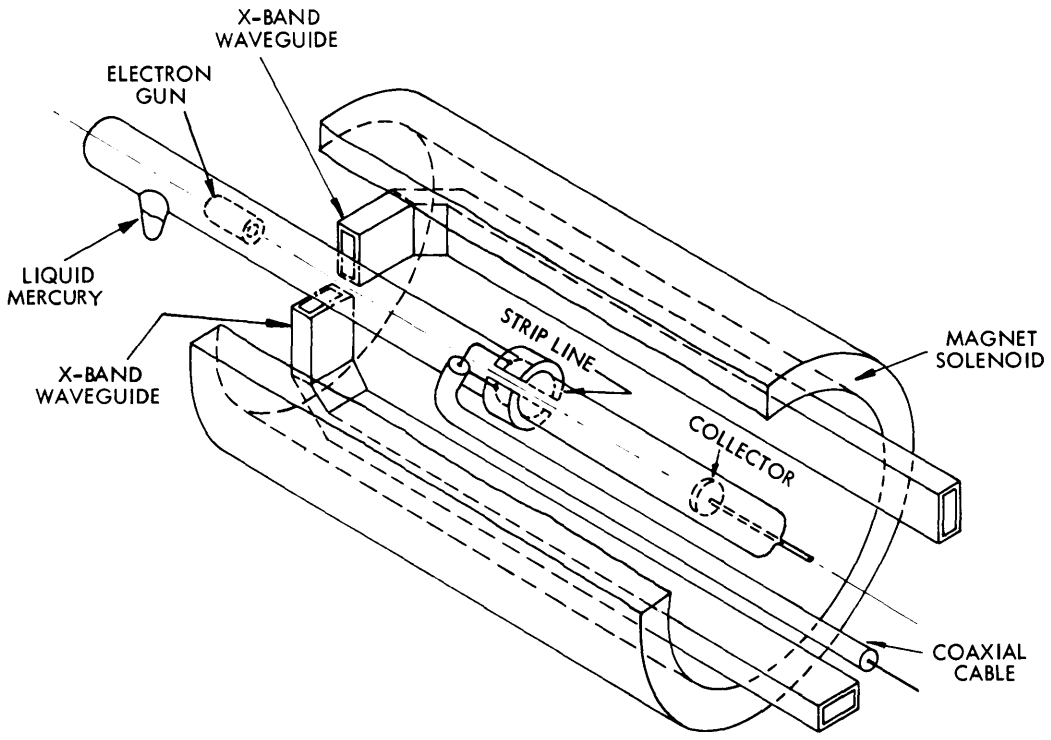

Fig. VII-13. Experimental geometry.

less than, the total beam velocity determined by the voltage applied to the electron gun.

The experimental geometry is shown in Fig. VII-13. Two open-ended pieces of X-band waveguide, which serve as microwave horns, enter the magnet solenoid and bend 90° to face the plasma tube. The horns are oriented so that the electric field for the lowest waveguide mode is parallel to the magnetic field. The horns are mounted on a movable structure so that their position along the axis of the tube can be varied. Displaced 11 cm along the axis from the horns is a strip-line antenna that couples capacitively to the plasma and picks up the plasma oscillations directly. The strip line is also mounted on the movable structure and moves along the axis with the horns.

The microwave circuit used in the scattering experiments is shown in Fig. VII-14.

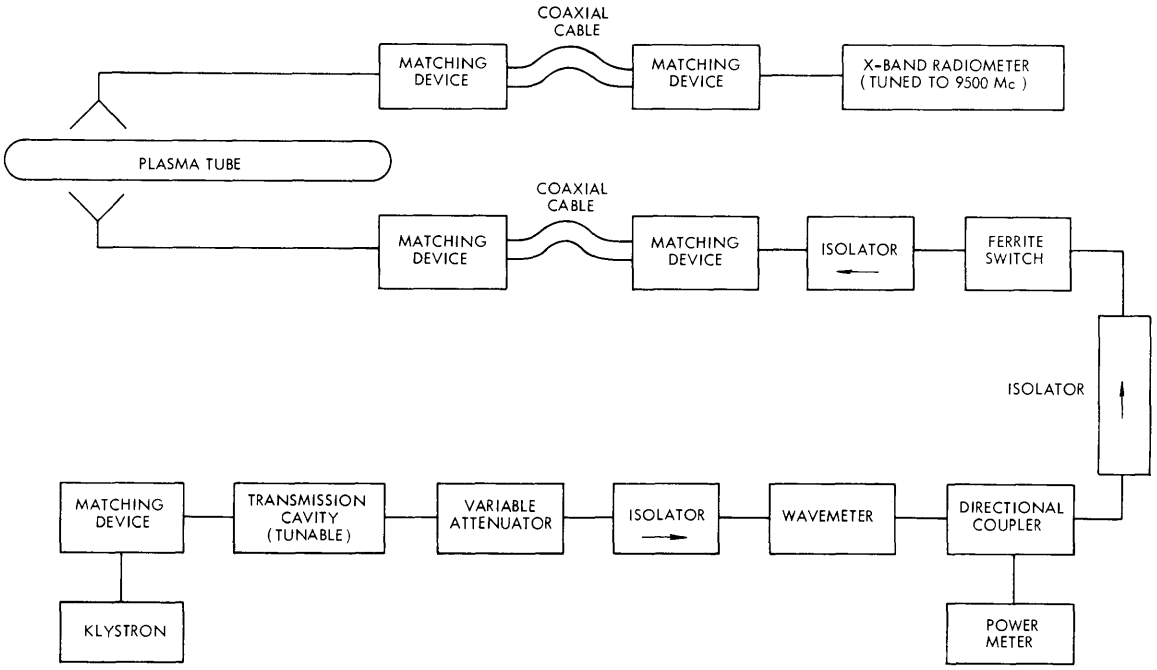

Fig. VII-14. Waveguide circuit.

Microwave radiation at frequency f_{inc} is incident on the plasma from one of the microwave horns. Scattered radiation is picked up by the other horn and fed to an X-band radiometer tuned to 9500 Mc. The amplitude of the scattered radiation at frequency f_{scat} = 9500 Mc is approximately proportional to the potential energy in the component of density fluctuations at the difference frequency $f_{scat} - f_{inc}$.

The scattered power was found to be roughly proportional to the incident power, which verified the fact that the effect is scattering of the incident radiation by the plasma, rather than direct emission at the radiometer frequency from the plasma. The scattered power was also found to vary greatly with the frequency of the incident radiation.

The electron beam is expected to interact with the plasma by the familiar two-stream instability mechanism to set up plasma waves along the axis of the tube, which could be reflected from the collector end of the tube and form standing waves. An attempt was therefore made to determine if standing waves existed along the axis of the tube. With the beam voltage and incident microwave power and frequency kept constant, the horns were moved along the axis of the tube. The support structure for the horns was moved by a screw and gear system, which also turned a small 10-turn potentiometer. This potentiometer was used to drive the x axis of an x-y recorder, and the output of the X-band radiometer was applied to the y axis of the recorder. The scattered power was then plotted against the axial position of the microwave horns. The result is shown in Fig. VII-15. The maxima and minima of the scattered power correspond to the maxima and minima of the density fluctuations, and these in turn represent the antinodes and nodes, respectively, of a standing plasma wave. The wavelength λ can be determined from the relation, $d = \lambda/2$, where d is the distance between nodes. The frequency of the standing wave is the difference between the frequencies of the scattered and incident microwaves. The phase velocity given by $v_p = \lambda f$ can then be calculated. We find that $\lambda = 3.6$ cm, $f = 232$ Mc, $v_p = 8.4 \times 10^8$ cm/sec. This is just 5 per cent less than the total beam velocity, which is 8.8×10^8 cm/sec. It seems quite clear that the scattering is from standing plasma waves excited by the electron beam.

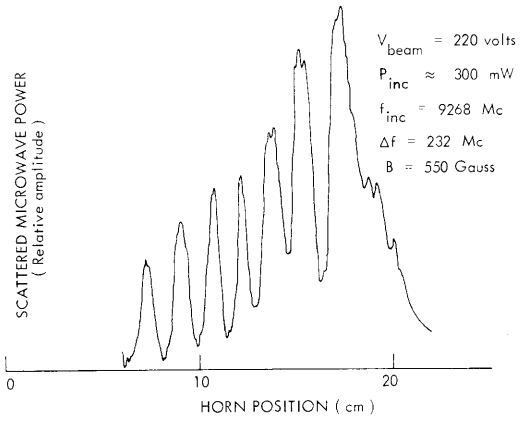

Fig. VII-15. Scattered microwave power vs horn position.

Further evidence for the existence of standing plasma waves along the axis of the tube was obtained by plotting the signal picked up by the strip-line antenna as a function of frequency. The strip line was connected by a coaxial cable to the input of a radio receiver and the output of the receiver is plotted against receiver frequency in Fig. VII-16. These data were taken at a lower magnetic field and a lower beam voltage than the scattering data presented in Fig. VII-15, so comparison with the scattering data is not possible. Figure VII-16 represents the spectrum of oscillations in the plasma and indicates that approximately 25 standing-wave modes are present in the plasma at one time. If we identify each peak with a mode number, n, where n is the number of half-wavelengths between the electron gun and the collector, then we can plot the frequency of the peaks against mode number, as shown in Fig. VII-17. It can be seen that the peaks are all equally spaced in frequency. This is to be expected for

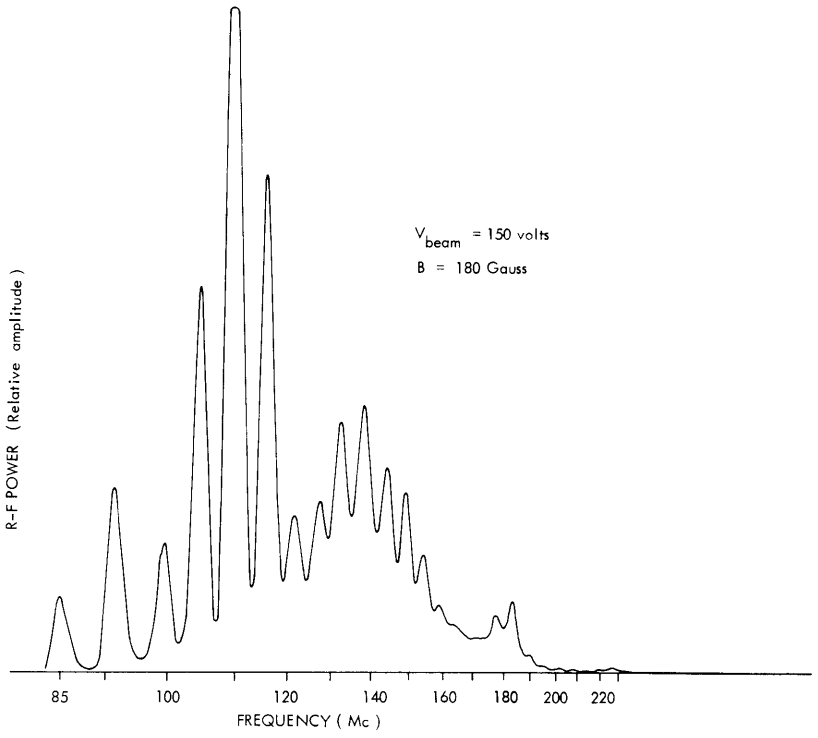

Fig. VII-16. RF power picked up by the strip line from the plasma vs frequency.

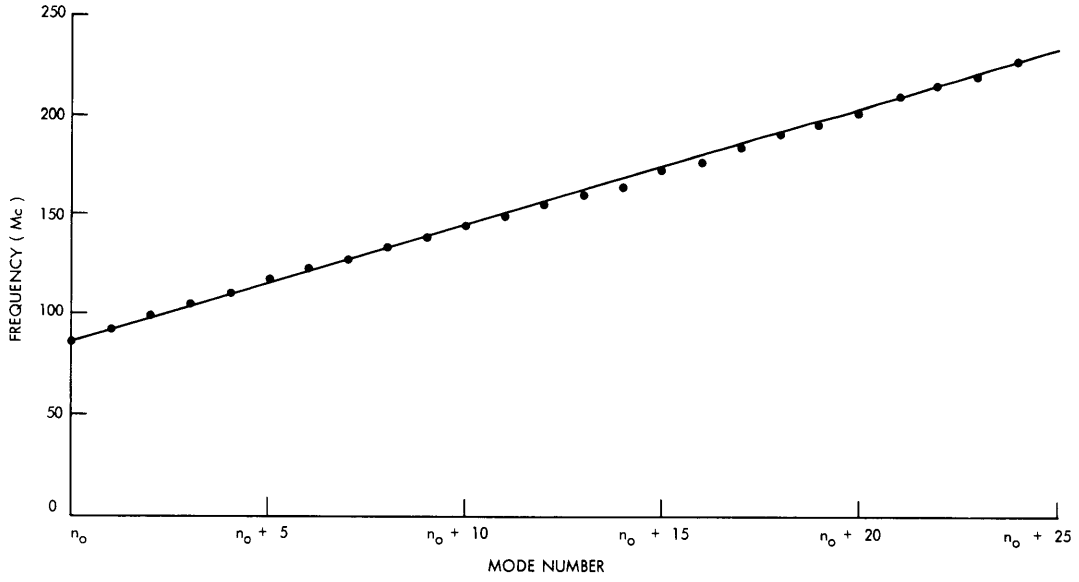

Fig. VII-17. Standing-wave frequency vs mode number.

standing waves that all have the same phase velocity, v_p, and wavelengths given by $D = n\lambda_n/2$, where D is the distance between the electron gun and the collector. Then $f_n = v_p/\lambda_n = nv_p/2D$. From Fig. VII-17 we note that the frequency separation f_n/n is 5.92 Mc. D is 42 cm. We can then calculate the phase velocity, $v_p = \lambda_n f_n = 4.96 \times 10^8$ cm/sec, which is approximately 30 per cent less than the total beam velocity, $v_{beam} = 7.3 \times 10^8$ cm/sec. This is not an unreasonable value for $v_$, the axial beam velocity, since part of the beam velocity is transverse.

A direct measurement of the axial wavelength of one of the standing wave modes shown in Fig. VII-16 was made by moving the strip line along the axis of the tube and

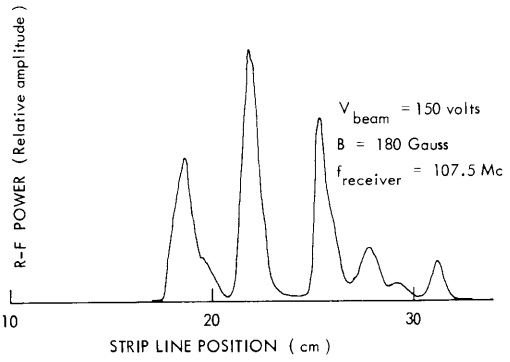

Fig. VII-18. RF power picked up by the strip line from the plasma vs strip-line position.

plotting the amplitude of the signal picked up from the plasma against axial position of the strip line. This is shown in Fig. VII-18. The periodic maxima and minima indicating antinodes and nodes of the standing wave are similar to those shown by the scattering in Fig. VII-15. In Fig. VII-18, however, the frequency of the wave is much lower than that in Fig. VII-15, so the wavelength is longer, and the nodes are more widely spaced. From Fig. VII-18 we get the axial wavelength, $\lambda = 6.30$ cm, and calculate the phase velocity, $v_p = \lambda f = 6.8 \times 10^8$ cm/sec. This is only 7 per cent less than the total beam velocity, which is 7.3×10^8 cm/sec.

It seems quite clear from the data presented here that the microwave scattering is from standing plasma waves excited by the electron beam, since axial movement of both the microwave horns and the strip line showed a standing-wave structure, and the experimentally measured phase velocity was equal to the total beam velocity within 7 per cent. The spectrum of oscillations picked up by the strip line shows that as many as 25 standing-wave modes can be present in the plasma at one time. The assumption that for the n^{th} mode, there are n half-wavelengths between the electron gun and the collector may be in error, since this assumption, together with the experimentally determined frequency difference between modes, implies a phase velocity 30 per cent less than the total beam velocity, which is in disagreement with the phase velocity measured

directly by axial movement of the horns and strip line.

R. L. Kronquist

References

1. R. L. Kronquist, "Microwave Scattering from an Electron-Beam Produced Plasma," Quarterly Progress Report No. 82, Research Laboratory of Electronics, M. I. T., July 15, 1966, pp. 109-114.